Dalton Transactions

PAPER

View Article Online
View Journal | View Issue

Cite this: *Dalton Trans.*, 2016, **45**, 5741

From molecular germanates to microporous Ge@C *via* twin polymerization†

Philipp Kitschke,[a] Marc Walter,[b,c] Tobias Rüffer,[d] Heinrich Lang,[d] Maksym V. Kovalenko[b,c] and Michael Mehring*[a]

Received 5th January 2016,
Accepted 24th February 2016

DOI: 10.1039/c6dt00049e

www.rsc.org/dalton

Four molecular germanates based on salicyl alcoholates, bis(dimethylammonium) tris[2-(oxidomethyl)phenolate(2-)]germanate (**1**), bis(dimethylammonium) tris[4-methyl-2-(oxidomethyl)phenolate(2-)]-germanate (**2**), bis(dimethylammonium) tris[4-bromo-2-(oxidomethyl)phenolate(2-)]germanate (**3**) and dimethylammonium bis[2-*tert*-butyl-4-methyl-6-(oxidomethyl)phenolate(2-)][2-*tert*-butyl-4-methyl-6-(hydroxymethyl)phenolate(1-)]germanate (**4**), were synthesized and characterized including single crystal X-ray diffraction analysis. In the solid state, compounds **1** and **2** exhibit one-dimensional hydrogen bonded networks, whereas compound **4** forms separate ion pairs, which are connected by hydrogen bonds between the dimethylammonium and the germanate moieties. The potential of these compounds for thermally induced twin polymerization (TP) was studied. Germanate **1** was converted by TP to give a hybrid material (**HM-1**) composed of phenolic resin and germanium dioxide. Subsequent reduction with hydrogen provided a microporous composite containing crystalline germanium and carbon (Ge@C – **C-1**, germanium content ~20%). Studies on **C-1** as an anode material for Li-ion batteries revealed reversible capacities of ~370 mA h $g_{Ge@C}^{-1}$ at a current density up to 1384 mA g^{-1} without apparent fading for 500 cycles.

1. Introduction

The concept of twin polymerization (TP), which is defined as a concerted formation of two polymers in one synthetic step starting from a single monomer,[1] provides a convenient approach for the synthesis of organic–inorganic hybrid materials (HM) such as polyfurfuryl alcohol/MO_x (MO_2 = Si,[2,3] Sn,[4] Ti,[5,6] Zr and Hf,[7] MO_3 = WO_3 [8]), poly(thiophene-2-methanol)/MO_2 (M = Sn,[4] and Ti[5]), phenolic resin/MO_x (MO_2 = Si,[9,10] Sn,[4] Zr and Hf,[7] MO_3 = WO_3,[8] MO_x = MO_2/SiO_2 with M = Sn,[11] Zr and Hf[7]), since it was reported in 2007 for the first time.[2] With regard to homogeneity of the materials, salicylic alcoholates of silicon were shown to be ideal precursors to provide nanostructured interpenetrating networks of the organic and inorganic components.[9,10] Such hybrid materials can be converted into highly porous carbon and/or metal oxide based materials depending on the reaction conditions. For instance, reduction of a tin-containing HM with hydrogen gave a porous Sn@C/SiO_2 material[11] accounting for the suitability of twin polymerization for the synthesis of metal containing porous carbon materials. Moreover, microporous carbon exhibiting BET surface areas up to 1260 m^2 g^{-1} are accessible by reduction of a material as obtained by polymerization of spirocyclic salicyl alcoholates of silicon and subsequent removal of SiO_2.[9,10] With this in mind, we anticipated that extension of the concept of TP to spirocyclic salicyl alcoholates of germanium may result in hybrid materials that can be converted into highly porous germanium-containing carbon materials (Ge@C). This class of compounds was shown to be interesting for applications as anode materials for Li-ion batteries (LIBs).[12–14] Such Ge@C materials should combine the advantages of germanium based materials *e.g.*, high gravimetric and volumetric capacity, high electrical conductivity and lithium-ion diffusivity, with enhanced cycling stability due to downsizing to the nanometer scale and incorporation into a carbon matrix as required for advanced anode materials for

[a]*Technische Universität Chemnitz, Fakultät für Naturwissenschaften, Institut für Chemie, Professur Koordinationschemie, 09107 Chemnitz, Germany. E-mail: michael.mehring@chemie.tu-chemitz.de*
[b]*Eidgenössische Technische Hochschule Zürich, Department of Chemistry and Applied Biosciences, Laboratory of Inorganic Chemistry, Vladimir-Prelog-Weg 1, 8093 Zürich, Switzerland*
[c]*Empa-Swiss Federal Laboratories for Materials Science and Technology, Laboratory for thin films and photovoltaics, Überlandstrasse 129, 8600 Dübendorf, Switzerland*
[d]*Technische Universität Chemnitz, Fakultät für Naturwissenschaften, Institut für Chemie, Professur Anorganische Chemie, 09107 Chemnitz, Germany*
† Electronic supplementary information (ESI) available. CCDC 1440864–1440866. For ESI and crystallographic data in CIF or other electronic format see DOI: 10.1039/c6dt00049e

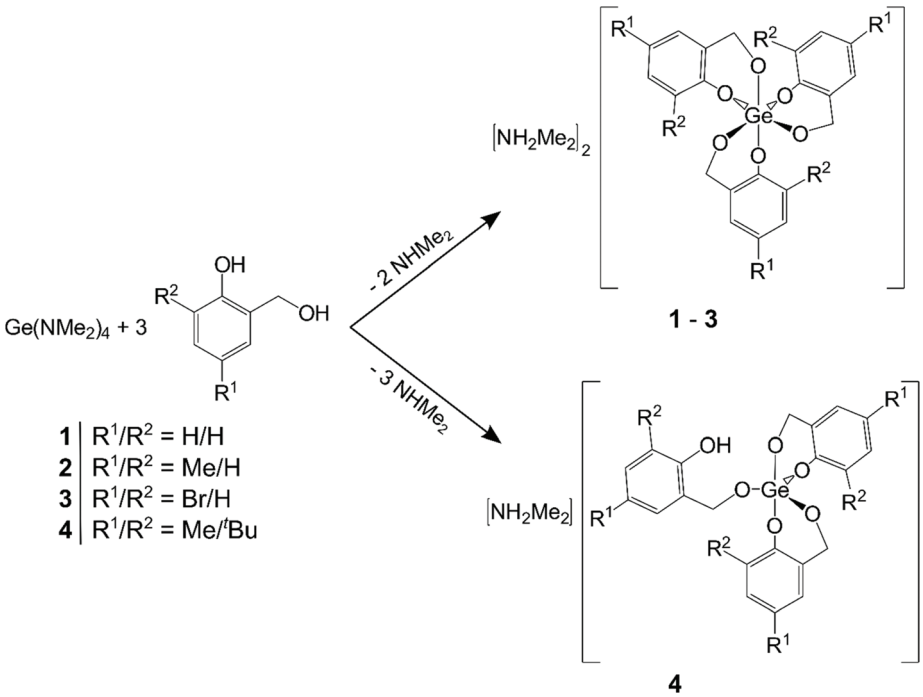

Scheme 1 Synthesis of the germanates **1–4** and illustration of the structural motifs of their anionic moieties.

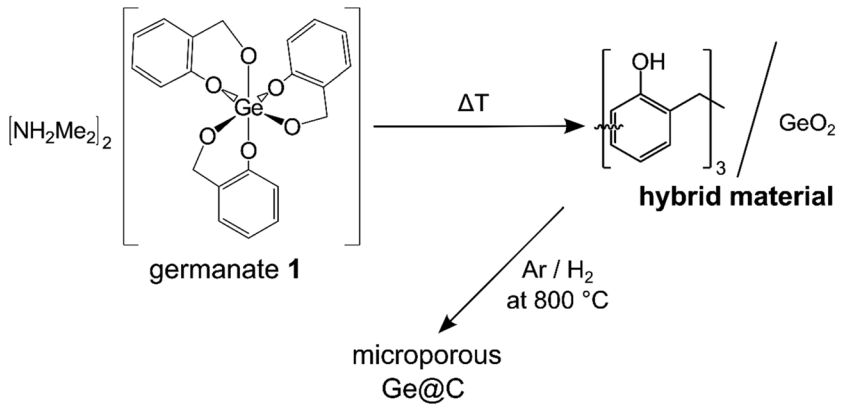

Scheme 2 Synthesis of a microporous Ge@C composite starting from germanate **1** following the concept of twin polymerization.

LIBs.[13,15–17] However, our attempts to synthesize spirocyclic salicyl alcoholates of germanium starting from germanium alkoxides and $GeCl_4$ failed.[18] Similarly, reactions of $Ge(NMe_2)_4$ with salicyl alcohols did not result in the germanium alcoholates, but gave the germanates **1–4** (Scheme 1).

These dimethylammonium germanates are the first representatives of anionic molecular precursors, which are potentially suitable for twin polymerization. Hence, in addition to their characterization we studied the reactivity of these compounds. Exemplarily, the as-prepared hybrid material as obtained from **1** was converted into microporous Ge@C following the synthetic concept as given in Scheme 2. In order to provide a proof of principle, the Ge@C composite was tested as anode material for rechargeable LIBs.

2. Results and discussion

2.1 Syntheses and characterization

The germanates **1–4** were synthesized starting from $Ge(NMe_2)_4$ and the respective salicyl alcohol with yields in the range of 64%–91% (Scheme 1). Good solubility in polar organic solvents was observed for the germanates **1**, **2** and **4**. Compound **4** is additionally soluble in nonpolar solvents such as *n*-hexane, whereas **3** is hardly soluble in polar organic solvents such as THF. The compounds were fully characterized including single crystal X-ray diffraction analysis for **1**, **2** and **4**. ^1H NMR, ^1H–^{13}C[19] HSQC and $^{13}C\{^1H\}$ NMR spectroscopic analyses of the germanates **1** and **2** in $CDCl_3$ gave two sets of resonance signals, respectively, at ambient temperature (Fig. S1

and S2†) that are assigned to the compounds **1** and **2** and species possessing a pentacoordinated anion. Temperature-dependent ^{1}H NMR spectroscopy exemplarily carried out for bis(dimethylammonium) tris[2-(oxidomethyl)phenolate(2-)] germanate (**1**) revealed an equilibrium between the two species with **1** being favored at lower temperatures (Fig. S3†). If the amount of $HNMe_2$ is varied these equilibriums between the hexacoordinated dianion and the pentacoordinated anion of the germanates will be shifted accordingly as was shown by ^{1}H NMR spectroscopy experiments exemplarily carried out for germanate **1** in $CDCl_3$ solution (Fig. S4†). Thus, the hexacoordinated compounds **1** and **2** show a dynamic behavior in solution to form an equilibrium with pentacoordinated species, respectively, in solution as illustrated in eqn (1). We propose that the pentacoordinated anions feature a similar structure (compounds **1a** and **2a**) to that of compound **4** (Scheme 1) in solution and in the solid state. However, isomers that exhibit bonding *via* the phenolic oxygen atom rather than *via* the benzylic oxygen atom cannot be completely ruled out on the basis of the NMR data. Notably, addition of a proton source to **1** and **2** induces decomposition rather than abstraction of a salicyl alcohol to give the neutral germanium alkoxide.

Single crystals suitable for X-ray diffraction analysis were obtained from saturated CH_2Cl_2 (**1** and **2**) and *n*-hexane (**4**) solutions by slow evaporation of the volatile solvents at ambient temperature. The compounds **1** and **2** show similar molecular structures of their dianions and their hydrogen bonded networks interconnecting the germanate dianions by dimethylammonium cations, whereas **4** exhibits a different structural motif of its anion in the solid state. Therefore, only the molecular structures of the germanates **1** and **4** are discussed. Details of the crystal structure of compound **2** (Fig. S8 and S9) are given in the ESI† and a summary of crystallographic data are presented in Table 1. Compound **1** possesses two crystallographically independent germanate dianions exhibiting Δ-{Δ-[Ge1(Sal)$_3$]$^{2-}$ with Sal = salicyl alcoholate(2-)} (Fig. 1) or Λ-configuration {Λ-[Ge2(Sal)$_3$]$^{2-}$} in the solid state (Fig. S10†). Selected bond lengths and bond angles of the compounds **1** and **2** are given in Tables S1–S3.†

The germanium atoms of the dianions of **1** are hexacoordinate by the oxygen atoms of the three salicyl alcoholate moieties with benzylic and phenolic oxygen atoms being opposite to each other to give a slightly distorted octahedral coordination geometry in both cases. The germanium oxygen bond lengths vary in the range from 1.879(2) to 1.911(2) Å for Δ-[Ge1(Sal)$_3$]$^{2-}$

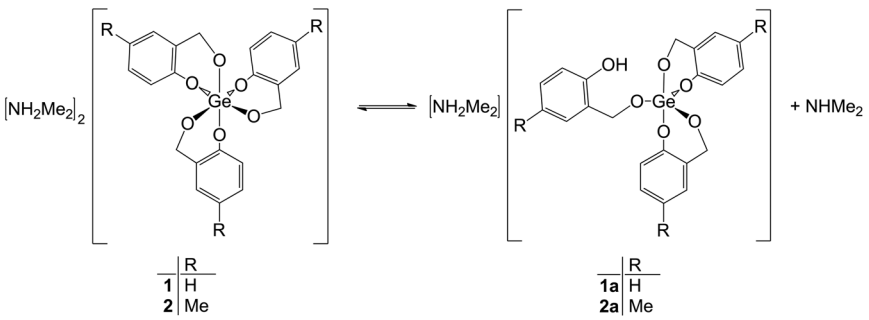

	R
1	H
2	Me

	R
1a	H
2a	Me

(1)

The ^{1}H NMR, ^{1}H–^{13}C{^{1}H} HSQC and ^{13}C{^{1}H} NMR spectra of compound **3** were recorded in [D$_8$]THF solution due to its poor solubility in other solvents. Two sets of resonance signals that are assigned to compound **3** and a pentacoordinated species (compound **3a**) were observed in the ^{1}H NMR spectrum at ambient temperature (Fig. S5†). In contrast to **1** and **2**, compound **3a** is assumed to be the dominant species in THF solution of **3** as indicated by the intensities of the resonance signals (Fig. S5†). One set of resonance signals was observed in the ^{1}H NMR, ^{1}H–^{13}C{^{1}H} HSQC and ^{13}C{^{1}H} NMR spectra, respectively, of germanate **4** (Fig. S6†). The multiplicity and the integral ratios of the resonance signals are in agreement with the structural motif of a pentacoordinated species as depicted in Scheme 1.

In the solid state, broad absorption bands assigned to ν N–H (2718 and 2462 cm^{-1} for **1**, 2732, 2462 and 2361 cm^{-1} for **2**, 2736 and 2448 cm^{-1} for **3** and 2460 cm^{-1} for **4**) vibrational modes were determined by attenuated total reflection (ATR) FT-IR spectroscopy for all germanates, whereas compound **4** gave an additional absorption band maximum at 3268 cm^{-1}, which was assigned to a ν O–H vibration (Fig. S7†).

and from 1.870(2) to 1.908(2) Å for Λ-[Ge2(Sal)$_3$]$^{2-}$ being in agreement with values reported for the dianions of dimethylammonium *fac*-tris[benzohydroximato(2-)]germanate·CH_3OH,[21] the germanium catecholato (cat = $C_6H_4O_2^{2-}$) complex, K_2[Ge(cat)$_3$]·3H_2O·2EtOH,[22] and the germanium enterobactin (Ent = 3,3′,3″-{[(2,6,10-trioxo-1,5,9-trioxacyclododecane-3,7,11-triyl)tris(azanediyl)]tris(carbonyl)}tris[benzene-1,2-bis(olate)]) complex, K_2[Ge(Ent)]·6DMF·H_2O.[23] Four dimethylammonium cations bind by hydrogen bonds of moderate strength[24] to the germanate dianion to give a one-dimensional, infinite hydrogen bonded network (Fig. S10 and Table S2†).

In contrast to the germanates **1** and **2**, a molecular ion pair of dimethylammonium cations and germanate anions was determined for **4** in the solid state due to presence of the sterically demanding *tert*-butyl group in *ortho* position of the salicyl alcoholate moieties. The molecular structure of **4** is depicted in Fig. 2 and selected bond lengths and bond angles are presented in Table S1.†

The germanium atom of compound **4** is pentacoordinated showing a distorted trigonal bipyramidal coordination sphere

Table 1 Crystallographic and experimental data of the single crystal X-ray diffraction analyses of **1**·1/2 CH_2Cl_2, **8**·**2**·17 CH_2Cl_2 and **4**

Compound	**1**·1/2 CH_2Cl_2	**8**·**2**·17 CH_2Cl_2	**4**
Formula	$C_{25.5}H_{35}ClGeN_2O_6$	$C_{241}H_{354}Cl_{34}Ge_8N_{16}O_{48}$	$C_{38}H_{57}GeNO_6$
Molecular mass	573.59 g mol^{-1}	6029.40 g mol^{-1}	696.43 g mol^{-1}
Temperature	110 K	110 K	110 K
Wavelength	1.54184 Å	0.71073 Å	0.71073 Å
Crystal system	Monoclinic	Triclinic	Triclinic
Space group	*I*2/*a*	*P*$\bar{1}$	*P*$\bar{1}$
Crystal size	0.1 × 0.04 × 0.01 mm	0.32 × 0.32 × 0.30 mm	0.3 × 0.3 × 0.3 mm
a	25.226(5) Å	13.5662(3) Å	10.5372(5) Å
b	20.080(3) Å	23.6439(6) Å	14.2260(8) Å
c	24.170(6) Å	24.7100(6) Å	14.3811(8) Å
α		69.244(2)°	118.392(6)°
β	120.32(3)°	79.577(2)°	92.482(4)°
γ		79.064(2)°	93.965(4)°
V	10 568(4) $Å^3$	7220.9(3) $Å^3$	1884.8(2) $Å^3$
Z	16	1	2
Density calculated	1.442 Mg m^{-3}	1.387 Mg m^{-3}	1.227 Mg m^{-3}
μ	2.864 mm^{-1}	1.204 mm^{-1}	0.856 mm^{-1}
F (000)	4784	3130	744
Theta range for data collection	3.054 to 63.747°	2.968 to 25.000°	3.228 to 24.999°
Index ranges	$-27 \le h \le 29$	$-16 \le h \le 16$	$-12 \le h \le 11$
	$-23 \le k \le 19$	$-28 \le k \le 28$	$-13 \le k \le 16$
	$-24 \le l \le 28$	$-29 \le l \le 29$	$-17 \le l \le 14$
Reflections collected	17 583	60 418	12 164
Independent reflections	8596 [*R*(int) = 0.0404]	25 388 [*R*(int) = 0.0268]	6621 [*R*(int) = 0.0181]
Data	8596	25 388	6621
Goodness-of-fit on F^2	1.009	1.037	1.064
Final *R* indices [$I > 2\sigma(I)$], ωR_2 (F^2) (all data)	R_1 = 0.0427, ωR_2 = 0.0991	R_1 = 0.0517, ωR_2 = 0.1349	R_1 = 0.0281, ωR_2 = 0.0709
Largest diff. peak and hole	0.584 and −0.533 e $Å^{-3}$	3.319 and −2.328 e $Å^{-3}$	0.363 and −0.273 e $Å^{-3}$

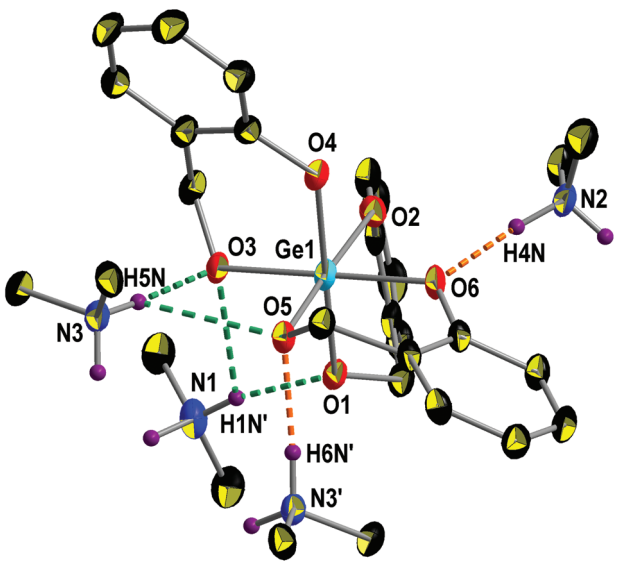

Fig. 1 Molecular structure of the dianion of **1** {Δ-[Ge1(Sal)$_3$]$^{2-}$} exhibiting Δ-configuration in the solid state together with four hydrogen bonded $[H_2NMe_2]^+$ cations. Thermal ellipsoids are drawn with 50% probability. All hydrogen atoms (ball and stick style) that are bonded to carbon atoms have been omitted for clarity. The intermolecular hydrogen bonding motifs C_2^2(**5**) (orange) and R_1^2(**4**) (green)[20] are depicted as dashed lines. Symmetry transformations used to generate equivalent atoms: ′ denotes $-x + 0.5, y, -z + 1$.

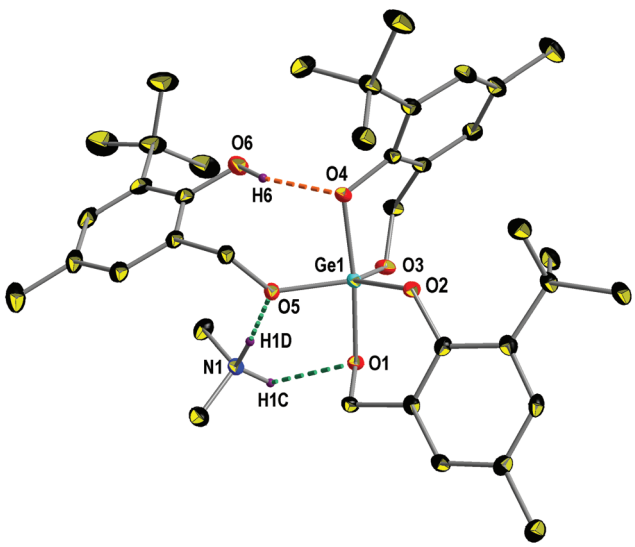

Fig. 2 Molecular structure of germanate **4** in the solid state. Thermal ellipsoids are drawn with 50% probability. All hydrogen atoms (ball and stick style) that are bonded to carbon atoms have been omitted for clarity. The intramolecular S (orange) and the intermolecular R_2^2(**6**) (green)[20] hydrogen bonding motifs are depicted as dashed lines.

by bonding to three benzylic (O1 in axial, O3 and O5 in equatorial positions) and two phenolic (O2 in equatorial and O4 in axial positions) oxygen atoms. The Ge–$O_{benzylic}$ bond lengths vary in the range from 1.7766(12) to 1.8435(11) Å, whereas the Ge–$O_{phenolic}$ distances [Ge1–O2 1.8025(11) Å and Ge1–O4 1.8844(11) Å] are slightly longer compared to Ge–$O_{benzylic}$ bond lengths with $O_{benzylic}$ located at equivalent positions (equatorial/axial). The bond lengths are in agreement with values reported for bis[citrate(2-)O^3,O^4](morpholiniomethyl)germanate

hydrate and *meso*-[1,4-piperaziniumdiylbis(methylene)]bis{bis-[2-methyllactato(2-)-O^1,O^2]germanate}·8H_2O.[25,26] The dimethylammonium cation and the germanate anion are bridged by hydrogen bonding [N1–O1 2.809(2) Å with N1–H1C–O1 being 159° and N1–O5 2.7718(18) Å with N1–H1D–O5 being 176°] of moderate strength[24] showing the $R_2^2(6)$ motif.[20] Moreover, an intramolecular hydrogen bond [O4–O6 2.826(2) Å with O4–H6–O6 being 163°] bridges the phenolic hydroxido group (O6) and the phenolic oxygen atom (O4) at axial position. Note that a phenol group rather than a benzyl alcohol group of the single coordinating salicyl alcoholate moiety is present in germanate **4**, which is remarkable, because the much higher acidity of phenol groups ($pK_s \approx 10$) in comparison with aliphatic hydroxyl groups ($pK_s \approx 15$) makes the phenol more reactive.[27] However, an intramolecular hydrogen bridge of the phenol group is formed, which stabilizes the observed isomer. As a result of this hydrogen bond bridge and the steric hindrance that is caused by the *tert*-butyl group, the determined structure is altogether energetically favored over the formation of the alternative isomer with the phenol group deprotonated and coordinated to the germanium atom, and exhibiting a hydrogen bond bridge of an aliphatic hydroxyl group.

2.2 Twin polymerization of germanate 1

Thermally induced TP of germanate **1** results in the formation of a hybrid material (HM) composed of phenolic resin/GeO_2 as illustrated in eqn (2) given for an idealized conversion of the starting material.

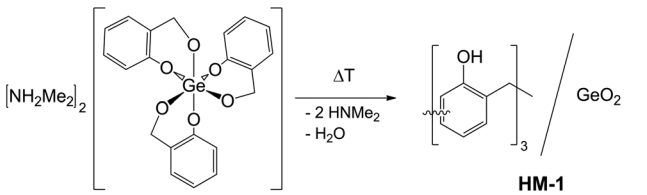

(2)

Bulk phase TP of compound **1** was carried out under inert atmosphere at 200 °C and gave an amorphous phenolic resin/GeO_2 hybrid material (**HM-1**) with a yield of 67% after the work-up procedure. The polymerization temperature was chosen according to the results of the differential scanning calorimetry (DSC) measurements (Fig. S11†). The germanates **1–3** show complex thermochemical behaviors upon heating exhibiting dominant exothermic processes with onset temperatures of 173 °C (**1**), 174 °C (**2**) and 180 °C (**3**), which are assigned to their polymerization. The onset temperatures are similar to those onset temperatures that were reported to initiate TP for the structurally related spirocyclic silicon salicyl alcoholates such as 4*H*,4′*H*-2,2′,spiro[benzo[*d*][1,3,2]dioxasiline] (196 °C).[9] Contrastingly to the latter class of silicon compounds, the germanates **1–3** do not melt. It is noteworthy that 2-[(dimethylamino)methyl]phenol is formed as a volatile byproduct of the TP process of **1** being in accordance with the experimentally determined higher weight loss of *ca.* 33% (bulk phase experiment: 33% and thermogravimetric analysis (TGA): 34% – Fig. S12†) as compared to the theoretically maximum weight loss of 20.7% due to the formation of $HNMe_2$ and water as indicated by the idealized eqn (2). **HM-1** was characterized by $^{13}C\{^1H\}$ cross polarization magic angle spinning (CP-MAS) NMR and ATR-FT-IR spectroscopy, powder X-ray diffraction (PXRD), CHN analysis and energy-dispersive X-ray (EDX) spectroscopy. The $^{13}C\{^1H\}$ CP-MAS NMR spectrum of **HM-1** is depicted in Fig. 3.

All expected resonance signals for a phenolic resin with typical chemical shifts as reported for hybrid materials obtained by thermally induced TP *e.g.*, of spirocyclic silicon salicyl alcoholates[9] were observed for **HM-1**. The intensive signals with chemical shifts centered at δ = 36 ppm, δ = 130 ppm and δ = 153 ppm show relatively small widths at half height. The latter and the chemical shifts that were determined for the bridging methylene groups *i.e.*, centered at δ = 36 ppm (*ortho*/*ortho*′ connectivity centered at δ = 30 ppm and *ortho*/*para*′ connectivity centered at δ = 35 ppm[28–30]), indicate that the phenolic resin possesses a prevailing *ortho*/*para*′ connectivity of the bridging methylene groups. However, the signal of lower intensity centered at δ = 120 ppm (unsubstituted carbon atoms in *para* position centered at δ = 120 ppm[28–30]) most likely originates from the presence of a minor secondary *ortho*/*ortho*′ connectivity pattern of the bridging methylene groups in **HM-1**. The broad signal of low intensity centered at δ = 43 ppm is assigned to a small portion of terminating CH_2NMe_2 groups that presumably result from incorporation of 2-[(dimethylamino)methyl]phenol, which is formed during the polymerization process as a byproduct.

Typical IR absorption bands for ν O–H (3600–3100 cm^{-1}), ν C=C (1590 cm^{-1}), ν C–O (1227 cm^{-1}), aromatic backbone vibrational modes (810 and 750 cm^{-1}) and Ge–O vibrational modes (451 and 506 cm^{-1}) were observed in the ATR-FT-IR spectra of **HM-1** (Fig. S13†). Additional absorption band maxima at 2361 cm^{-1} (ν N–H) and 1096 cm^{-1} (ν N–C) were assigned and are in accordance with the presence of CH_2NMe_2 groups. CHN analysis gave carbon, hydrogen and nitrogen

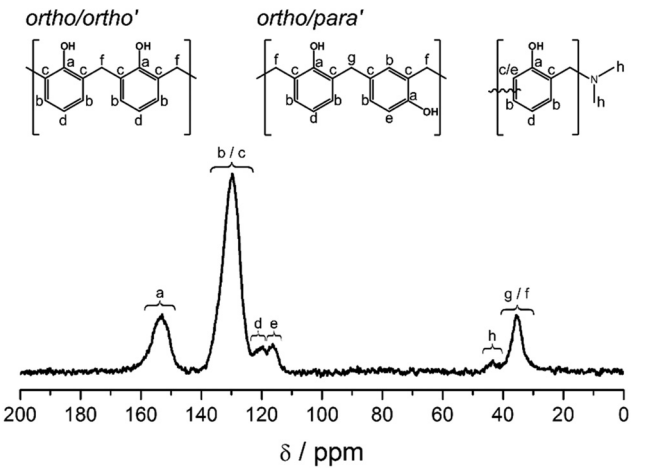

Fig. 3 $^{13}C\{^1H\}$ CP-MAS NMR spectra of **HM-1** given with assignment of the resonance signals.

contents of 53.8%, 4.9% and 2.6%, respectively, that differ from the expected values (C, 59.6% and H, 4.3%) as calculated for the idealized composition based on eqn (2). However, the latter is in agreement with the formation of 2-[(dimethylamino)methyl]phenol as byproduct and its partial incorporation into the HM during the polymerization process. This is further supported by EDX analysis of **HM-1** [N, (5.0 ± 1.7)%].

2.3 Synthesis and characterization of the porous materials

Conversion of **HM-1** under oxidative conditions gave crystalline hexagonal GeO_2 exhibiting an adsorption isotherm assigned to type II (Fig. S14†) with a BET surface area of 27 $m^2\ g^{-1}$, which is indicative for the formation of non-porous GeO_2. A microporous material consisting of germanium and carbon (Ge@C material **C-1**) was obtained by conversion of **HM-1** under reducing conditions (Ar/H_2 95/5) at 800 °C (Scheme 2). Analysis of the adsorption isotherm, which is assigned to a type I isotherm (Fig. S14†) using a QSDFT model for slit and cylindrical pores, revealed a micropore content of 61% with a BET surface area of 470 $m^2\ g^{-1}$. A CHN analysis revealed a carbon content of 59.6%, which is slightly increased compared to the carbon contents of the pristine compound **1** (56.5%) and **HM-1** (53.8%). A germanium content of (20.5 ± 1.0)% was detected for **C-1** by EDX analysis. Crystalline germanium particles with average primary particle sizes of (27 ± 1) nm were determined based on PXRD analysis (Fig. S15†). Raman spectroscopy using a confocal micro Raman system revealed areas for **C-1** that exhibit high germanium but low carbon contents and areas of high carbon but low germanium contents (Fig. S16†). The latter is indicative that both germanium-enriched and carbon-enriched domains ranging up to the μm-scale were formed during the formation of **C-1** due to sintering processes of the germanium particles at higher temperatures (>600 °C).

2.4 Electrochemical measurements

In order to provide a proof of principle, **C-1** was tested as potential anode material for rechargeable Li-ion batteries. Electrodes with carbon black (CB) as conductive additive and carboxymethylcellulose (CMC) as binder were prepared with a ratio of 80 : 10 : 10. The electrode was tested in Li-ion half cells with 1 M $LiPF_6$ in a mixture (1 : 1 by weight) of ethylene carbonate (EC) and dimethylcarbonate (DMC) as electrolyte. Further, fluoroethylene carbonate (FEC) was added to the electrolyte to improve cycling stability.[31] The electrochemical tests using **C-1** as electrode material are shown in Fig. 4. Currents and capacities are given related to the mass of **C-1** (Ge@C).

At both current densities of 346 mA $g_{Ge@C}^{-1}$ and 1384 mA $g_{Ge@C}^{-1}$ (corresponding to approximately 1C and 4C given the actual capacity of the material) no fading is observed for 100 and 500 cycles, respectively, with capacities of ~370 mA h $g_{Ge@C}^{-1}$. Due to the large surface area and therefore high irreversible charge loss caused by the solid electrolyte interface (SEI) formation the coulombic efficiency in all cases is only ~25% in the first cycle, but increases to ≥99% during subsequent cycling. The irreversible charge loss during the first discharge is further apparent by the peak at 0.4 V *vs.* Li^+/Li

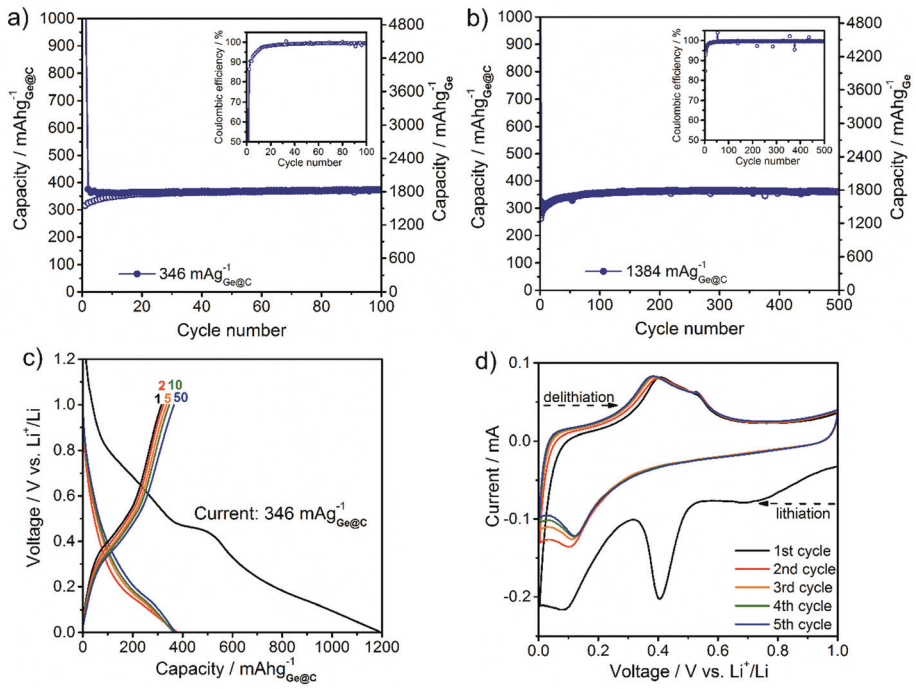

Fig. 4 Electrochemical performance of **C-1** as anode material for Li-ion batteries. Capacities and currents are either related to the whole **C-1** (Ge@C) composite or only to the fraction of germanium excluding carbon. (a) Cycling stability at a current of 346 mA $g_{Ge@C}^{-1}$. (b) Cycling stability at a current of 1384 mA $g_{Ge@C}^{-1}$. (c) Galvanostatic charge and discharge curves of at a current of 346 mA $g_{Ge@C}^{-1}$. (d) Cyclic voltammogram of **C-1** at a scan rate of 0.1 mV s^{-1}. All cells were cycled in the potential range 0.005–1.0 V.

observed in the cyclic voltammogram (Fig. 4d). EDX analysis gave a germanium content of (20.5 ± 1.0)% for **C-1**. In the light of the low germanium content, the porous Ge@C material as-prepared starting from a TP process holds considerable potential as high-performance anode material for rechargeable LIBs with respect to its excellent cycling stability and rate capability.

3. Conclusions

The molecular germanates bis(dimethylammonium) tris-[2-(oxidomethyl)phenolate(2-)]germanate (**1**), bis(dimethylammonium) tris[4-methyl-2-(oxidomethyl)phenolate(2-)]germanate (**2**), bis(dimethylammonium) tris[4-bromo-2-(oxidomethyl)-phenolate(2-)]germanate (**3**) and dimethylammonium bis-[2-*tert*-butyl-4-methyl-6-(oxidomethyl)phenolate(2-)][2-*tert*-butyl-4-methyl-6-(hydroxymethyl)phenolate(1-)]germanate (**4**) were synthesized, which are composed of either germanate dianions with hexacoordinated germanium atoms (**1–3**) or of a germanate anion exhibiting a trigonal bipyramidal coordination of the germanium atom (**4**) in the solid state. NMR spectroscopic analyses revealed that the germanates **1–3** are in an equilibrium in solution between their dianionic structure as determined in the solid state and species possessing pentacoordinated anions that feature a similar structure as the anion of **4**. Germanate **4** does not form such an equilibrium in solution most presumably due to the steric hindrance of its *tert*-butyl groups in *ortho* position at the salicyl alcoholate moieties. Single crystal X-ray diffraction analysis revealed hydrogen bonds between the dimethylammonium cations and the germanates resulting in one-dimensional, infinite hydrogen bridged networks within chains formed by the dimethylammonium cations and germanate dianions for the racemic crystals of the compounds **1** and **2**. Molecular ion pairs of the dimethylammonium cation and the germanate anion were observed in case of the racemate **4** in the solid state. Thermally induced twin polymerization of compound **1** gave a hybrid material, which is composed of a phenolic resin and GeO_2. The latter was converted into either microporous Ge@C under reducing conditions or crystalline hexagonal GeO_2 under oxidative conditions. An excellent cycling stability and rate capability were observed upon first tests of the as-obtained Ge@C composite as anode material in LIBs. Although the effective capacity of ~370 mA h $g_{Ge@C}^{-1}$ is only moderate, which is attributed to the low germanium content of ~20% within the Ge@C material, the results concerning cycling stability are promising. We demonstrated for the first time that the approach of twin polymerization can be applied to anionic molecular precursors and without the need for any catalyst. The reduction process offers a convenient way towards microporous Ge@C composites. However, increasing the germanium content and/or graphitizing the carbon matrix will be a prerequisite for further developments of this approach with regard to high performance anode materials and is currently under investigation.

4. Experimental section

All reactions were performed under argon using Schlenk techniques or in a glovebox. Solvents were purified and dried by applying standard techniques. The reactions were carried out with freshly distilled, anhydrous solvents. ^{1}H, $^{13}C\{^{1}H\}$ and ^{1}H-$^{13}C\{^{1}H\}$ HSQC NMR spectra were recorded with a Bruker Avance III 500 spectrometer. Solid state NMR spectra were collected at 9.4 T with a Bruker Avance 400 spectrometer equipped with double-tuned probes capable of magic angle spinning (MAS). $^{13}C\{^{1}H\}$ CP MAS NMR spectra were measured at 100.6 MHz in 3.2 mm standard zirconium oxide rotors (BRUKER) spinning at 20 kHz. Cross polarization (CP) with a contact time of 3 ms was used to enhance sensitivity. The recycle delay was 5 s. The spectrum was referenced externally to tetramethylsilane (TMS) as well as to adamantane as secondary standard (38.48 ppm for ^{13}C). All spectra were collected with ^{1}H decoupling using a two-pulse phase modulation sequence. ATR-FT-IR spectra were recorded with a BioRad FTS-165 spectrometer. Raman spectra were collected on a LabRam HR800 confocal micro Raman system equipped with a Helium–Neon-laser (λ = 632.8 nm, P = 3.08 mW) without usage of any filter (D0) at fiftyfold magnification. Energy-dispersive X-ray spectroscopy (EDX) was performed using a Nova-Nano SEM from FEI with the following parameters: pressure (~10^{-5} mbar), work distance (5 to 7 mm) and acceleration voltage (18 kV) using a Si Drift Detector XFlash 3001 from Bruker AXS. Melting points were determined with a Melting Point B-540 apparatus from Büchi. CHN analyses were determined using a FlashEA 1112 NC Analyzer from Thermo Fisher Scientific. DSC experiments were determined with a Mettler Toledo DSC 30 using 40 μL aluminum crucibles. The measurements were performed up to 300 °C with a heating rate of 10 K min^{-1} in N_2 atmosphere and a volume flow of 50 mL min^{-1}. TGA experiments were determined with a Mettler Toledo TGA/DSC1 1600 system with an MX1 balance. The measurement was performed from 40 to 800 °C with a heating rate of 10 K min^{-1} in Ar atmosphere and a volume flow of 60 mL min^{-1}. Nitrogen physisorption isotherms were obtained at −196 °C using an Autosorb IQ2 apparatus from Quantachrome. All samples were activated in vacuum at 150 °C for 3 h prior to the measurements. Specific surface areas were calculated applying the BET equation (p/p_0 = 0.150 ± 0.002). The micropore content was estimated according to a QSDFT model (QSDFT: Quenched Solid Density Functional Theory, model for slit and cylindrical pores using the adsorption branch) for carbon samples using the Autosorb 1.56 software from Quantachrome.[32–39] The specific micropore and total pore volume were also calculated by the above mentioned DFT models. Powder X-ray diffraction (PXRD) patterns were collected using a STOE STADI P diffractometer from STOE with Cu-K_α radiation (40 kV, 40 mA) and a Ge(111) monochromator. The crystallite size was estimated using the Scherrer equation: $\tau = K\lambda/\beta\cos\theta$, where τ is the volume weighted crystallite size, K is the Scherrer constant here taken as 1.0, λ is the X-ray wavelength, θ is the Bragg angle in ° and β is the full width of the

diffraction line at half of the maximum intensity (FWHM, background subtracted). The FWHM is corrected for instrumental broadening using a LaB_6 standard (SRM 660) purchased from NIST (National Institute of Standards and Technology). The value of β was corrected from ($\beta_{measured}{}^2$ and $\beta_{instrument}{}^2$ are the FWHMs of measured and standard profiles):

$$\beta^2 = \beta_{measured}{}^2 - \beta_{instrument}{}^2.$$

Germanium(IV) chloride was purchased from ABCR GmbH & Co KG. 2.5 M *n*-butyllithium, 2-*tert*-butyl-4-methylphenol and 5-bromo-2-hydroxybenzaldehyde were purchased from Merck Schuchardt OHG (Hohenbrunn). 2-Hydroxybenzyl alcohol, 4-methylphenol and dimethylamine (2 M solution in THF) were purchased from Alfa Aesar GmbH & Co KG (Karlsruhe). 3-*tert*-butyl-2-hydroxy-5-methylbenzyl alcohol,[9] $LiNMe_2$,[40] $Ge(NMe_2)_4$,[41] 2-hydroxy-5-methylbenzaldehyde,[42] 2-hydroxy-5-methylbenzyl alcohol[9] and 5-bromo-2-hydroxybenzyl alcohol[9] were synthesized according to literature procedures. 2-Hydroxybenzyl alcohol was purified by column chromatography (on silica gel using an ethyl acetate/*n*-hexane (ratio 20/80, v/v) mixture as eluent) before usage.

4.1 Synthesis of bis(dimethylammonium) tris[2-(oxidomethyl)phenolate(2-)]germanate (1)

A solution of $Ge(NMe_2)_4$ (0.769 g, 3.09 mmol) in diethyl ether (5 mL) was added dropwise into a solution of 2-hydroxybenzyl alcohol (1.150 g, 9.27 mmol) in diethyl ether (45 mL) at −60 °C. The mixture was stirred and allowed to reach ambient temperature. The precipitate was filtered off and washed with *n*-pentane (3 times 5 mL) to give germanate **1** as colorless solid after evaporating the volatile residues under reduced pressure (10^{-2} mbar). Yield: 1.507 g, 91%; decomposition 103–123 °C (with release of volatile products to give a yellow liquid); ^{1}H NMR (500 MHz, $CDCl_3$, 25 °C, TMS): δ = 1.52 (s, 9.33 H, CH_3), 2.46 [s (broad), 0.27 H, CH_3], 3.86 (d, 3 H, CH_2, ^2J = 12.9 Hz), 5.51 (d, 3 H, CH_2, ^2J = 12.9 Hz), 6.46 [d (broad), 3 H, C_6H_4, $^3J \sim$ 7.9 Hz], 6.54 [t (broad), 3 H, C_6H_4, $J \sim$ 7.3 Hz], 6.73 [t (broad), 3 H, C_6H_4, $J \sim$ 7.0 Hz], 6.94 [d (broad), 3 H, C_6H_4, $J \sim$ 7.6 Hz], 7.80 [s (broad), 1 H, NH_2], 9.52 ppm [s (broad), 3 H, NH_2)]; ^{13}C{^{1}H} NMR (125 MHz, $CDCl_3$, 25 °C, TMS): δ = 33.3 (*C*H$_3$), 60.0 (*C*H$_2$), 115.9 (C_6H$_4$), 119.3 (C_6H$_4$), 125.6 (C_6H$_4$), 128.4 (C_6H$_4$), 131.1 (C_6H$_4$), 161.3 ppm (C_6H$_4$); ^{1}H ^{13}C{^{1}H} HSQC NMR (125 MHz, $CDCl_3$, 25 °C, TMS): δ = 1.52/33.3 (*C*H$_3$), 2.46/36.1 (*C*H$_3$), 3.86/66.2 (*C*H$_2$), 5.51/66.2 (*C*H$_2$), 6.46/119.4 (C_6H_4), 6.54/116.1 (C_6H_4), 6.73/125.8 (C_6H_4), 6.94/128.5 ppm (C_6H_4); NMR analysis data for **1a**: ^{1}H NMR (500 MHz, $CDCl_3$, 25 °C, TMS): δ = 2.46 [s (broad), 12 H, CH_3], 4.52/4.64/4.77 [3 s (broad), 6 H, CH_2], 5.90–7.20 [m (broad), 12 H + 2*1 H, C_6H_4, O*H*, N*H*/NH_2], 7.80 ppm [s (broad), 2 H, N*H*/NH_2]; ^{13}C{^{1}H} NMR (125 MHz, $CDCl_3$, 25 °C, TMS): δ = 36.0 (*C*H$_3$), 60.3 ppm (*C*H$_2$); ^{1}H ^{13}C{^{1}H} HSQC NMR (125 MHz, $CDCl_3$, 25 °C, TMS): δ = 2.46/36.1 (*C*H$_3$), 4.52/66.4 (*C*H$_2$), 4.64/66.4 (*C*H$_2$), 4.77/66.4 (*C*H$_2$), 6.54/118.3 (C_6H_4), 6.59/118.1 (C_6H_4), 6.51/125.6 (C_6H_4), 6.72/116.2 ppm (C_6H_4); ATR-FT-IR: 3002 (ν C_{aryl}–H), 2961 (ν CH_2), 2850 (ν CH_2), 2718 (ν N–H), 2462 (ν N–H), 1648 (ν C=C), 1596 (ν C=C), 1575 (ν C=C), 1478 (δ CH_2), 1451 (δ CH_2), 1262 (ν C–O), 1198 (ν C–O), 1109 (ν C–N), 1013 (ν C–C), 754 (γ C_6H_4), 727 (γ C_6H_4), 596 (ν Ge–O), 556 and 517 and 486 and 419 cm^{-1} (O–Ge–O/Ge–O–Ge); single crystals suitable for X-ray diffraction analysis were obtained by slow evaporation of the solvent at ambient temperature of a saturated solution of **1** in CH_2Cl_2 to give **1**·1/2 CH_2Cl_2. CHN analysis calcd (%) for **1**·1/2 CH_2Cl_2 ($C_{25.5}H_{35}GeClN_2O_6$): C, 53.4; H, 6.2; N, 4.9; found: C, 53.8; H, 6.2; N, 4.6.

4.2 Synthesis of bis(dimethylammonium) tris[4-methyl-2-(oxidomethyl)phenolate(2-)]germanate (2)

A solution of $Ge(NMe_2)_4$ (0.540 g, 2.17 mmol) in diethyl ether (15 mL) was added dropwise into a solution of 2-hydroxy-5-methylbenzyl alcohol (0.898 g, 6.51 mmol) in diethyl ether (60 mL) at −40 °C. The mixture was stirred and allowed to reach ambient temperature. The precipitate was filtered off and washed with *n*-pentane (3 times 5 mL) to give germanate **2** as colorless solid after evaporating the volatile residues under reduced pressure (10^{-2} mbar). Yield: 1.012 g, 81%; decomposition 102–116 °C (with release of volatile products to give a colorless viscous substance); ^{1}H NMR (500 MHz, $CDCl_3$, 25 °C, TMS): δ = 1.56 (s, 9.08 H, NCH_3), 2.18 [s (broad), 9 H, CH_3], 2.41 [s (broad), 0.87 H, NCH_3], 3.83 (d, 3 H, CH_2, ^2J = 12.9 Hz), 5.50 (d, 3 H, CH_2, ^2J = 12.9 Hz), 6.43 [d (broad), 3 H, C_6H_3, $^3J_{ortho}$ = 7.9 Hz], 6.56 [s (broad), 3 H, C_6H_3], 6.76 [d (broad), 3 H, C_6H_3, $^3J_{ortho}$ = 7.9 Hz], 7.30 [s (broad), 1 H, NH_2], 9.61 ppm [s (broad), 3 H, NH_2)]; ^{13}C{^{1}H} NMR (125 MHz, $CDCl_3$, 25 °C, TMS): δ = 20.5 (*C*H$_3$), 33.5 (NCH_3), 66.0 (*C*H$_2$), 118.9 (C_6H_3), 124.6 (C_6H_3), 126.2 (C_6H_3), 128.6 (C_6H_3), 130.7 (C_6H_3), 158.8 ppm (C_6H_3); ^{1}H ^{13}C{^{1}H} HSQC NMR (125 MHz, $CDCl_3$, 25 °C, TMS): δ = 1.56/33.4 (NCH_3), 2.19/20.5 (*C*H$_3$), 2.42/36.4 (NCH_3), 3.75/66.0 (*C*H$_2$), 5.42/66.0 (*C*H$_2$), 6.34/118.7 (C_6H_3), 6.47/126.1 (C_6H_3), 6.67/128.7 ppm (C_6H_3); NMR analysis data for **2a**: ^{1}H NMR (500 MHz, $CDCl_3$, 25 °C, TMS): δ = 2.18 [s (broad), 9 H, CH_3], 2.41 [s (broad), 12 H, NCH_3], 4.58/4.66/4.73 [3 s (broad), 6 H, CH_2], 5.90–7.00 [m (broad), 12 H + 1 H, C_6H_4, O*H*], 7.80 ppm [s (broad), 3 H, N*H*/NH_2]; ^{13}C{^{1}H} NMR (125 MHz, $CDCl_3$, 25 °C, TMS): δ = 20.4 (*C*H$_3$), 36.3 ppm (NCH_3); ^{1}H ^{13}C{^{1}H} HSQC NMR (125 MHz, $CDCl_3$, 25 °C, TMS): δ = 2.19/20.4 (*C*H$_3$), 2.42/36.4 (NCH_3), 4.58/66.2 (*C*H$_2$), 4.65/64.1 (*C*H$_2$), 6.34/114.7 (C_6H_3), 6.40/117.9 (C_6H_3), 6.55/128.4 ppm (C_6H_3); ATR-FT-IR: 2990 (ν C_{aryl}–H), 2961 (ν CH_3/CH_2), 2913 (ν CH_3/CH_2), 2855 (ν CH_3/CH_2), 2732 (ν N–H), 2462 (ν N–H), 2361 (ν N–H), 1544 (ν C=C), 1611 (ν C=C), 1572 (ν C=C), 1487 (δ CH_3/CH_2), 1420 (δ CH_3/CH_2), 1266 (ν C–O), 1221 (ν C–O), 1144 (ν C–N), 1127 (ν C–N), 1024 (ν C–C), 999 (ν C–C), 822 (γ C_6H_3), 799 (γ C_6H_3), 554 and 509 and 482 and 420 cm^{-1} (O–Ge–O/Ge–O–Ge). Single crystals suitable for X-ray diffraction analysis were obtained by slow evaporation of the solvent at ambient temperature of a saturated solution of **2** in CH_2Cl_2 to give 8·**2**·17 CH_2Cl_2. CHN analysis of the crystals after evaporating volatile residues under reduced pressure (10^{-2} mbar) calcd (%) for **2**·CH_2Cl_2 ($C_{29}H_{42}GeCl_2N_2O_6$): C, 52.9; H, 6.4; N, 4.3; found: C, 52.8; H, 6.4; N, 3.7.

4.3 Synthesis of bis(dimethylammonium) tris[4-bromo-2-(oxidomethyl)phenolate(2-)]germanate (3)

A solution of $Ge(NMe_2)_4$ (0.480 g, 1.93 mmol) in diethyl ether (15 mL) was added dropwise into a solution of 5-bromo-2-hydroxybenzyl alcohol (1.173 g, 5.79 mmol) in diethyl ether (60 mL) at −40 °C. The mixture was stirred and allowed to reach ambient temperature. The precipitate was filtered off and washed with diethyl ether (3 times 5 mL) to give germanate **3** as colorless solid after evaporating the volatile residues under reduced pressure (10^{-2} mbar). Yield: 1.235 g, 83%; decomposition 146–152 °C (with release of volatile products to give an orange viscous substance); ^{1}H NMR (500 MHz, [D$_8$]THF, 25 °C, TMS): δ = 2.39 [s (broad), 12 H, CH_3], 4.76 [m (broad), 6 H, CH_2], 6.44–7.40 [m (broad), 9 H, C$_6H_3$], 8.00 ppm [s (broad), 4 H, NH/NH_2]; NMR analysis data for **3a**: ^{1}H NMR (500 MHz, [D$_8$]THF, 25 °C, TMS): δ = 2.39 [s (broad), 12 H, CH_3], 4.60 (s, 6 H, CH_2), 6.60 [d (broad), 3 H, C$_6H_3$, $^3J_{ortho}$ = 8.5 Hz], 6.87 [s (broad), 1 H, OH], 7.13 [dd (broad), 3 H, C$_6H_3$, $^3J_{ortho}$ = 8.5 Hz, $^4J_{meta}$ = 2.2 Hz], 7.39 [d (broad), 3 H, C$_6H_3$, $^4J_{meta}$ = 2.2 Hz], 8.00 ppm [s (broad), 3 H, NH/NH_2]; ^{13}C{^{1}H} NMR (125 MHz, [D$_8$]THF, 25 °C, TMS): δ = 35.2 (CH_3), 60.9 (CH_2), 112.0 (C$_6H_3$), 117.5 (C$_6H_3$), 130.7 (C$_6H_3$), 131.0 (C$_6H_3$), 132.0 (C$_6H_3$), 155.3 ppm (C$_6H_3$); ^{1}H ^{13}C{^{1}H} HSQC NMR (125 MHz, [D$_8$]THF, 25 °C, TMS): δ = 2.40/36.8 (CH_3), 4.60/60.9 (CH_2), 6.60/117.5 (C$_6H_3$), 7.13/131.0 (C$_6H_3$), 7.39/130.7 ppm (C$_6H_3$);ATR-FT-IR: 3014 (ν C$_{aryl}$–H), 2958 (ν CH$_2$), 2902 (ν CH$_2$), 2851 (ν CH$_2$), 2736 (ν N–H), 2448 (ν N–H), 1646 (ν C═C), 1586 (ν C═C), 1561 (ν C═C), 1466 (δ CH$_2$), 1408 (δ CH$_2$), 1262 (ν C–O), 1183 (ν C–N), 1119 (ν C–N), 1073 (ν C–Br), 1021 (ν C–C), 814 (γ C$_6$H$_3$), 781 (γ C$_6$H$_3$), 646 (ν Ge–O), 552 and 523 and 494 and 419 cm^{-1} (O–Ge–O/Ge–O–Ge); CHN analysis calcd (%) for **3** (C$_{25}$H$_{31}$Br$_3$GeN$_2$O$_6$): C, 39.1; H, 4.1; N, 3.7; found: C, 39.2; H, 4.1; N, 3.2.

4.4 Synthesis of dimethylammonium bis[2-*tert*-butyl-4-methyl-6-(oxidomethyl)phenolate(2-)][2-*tert*-butyl-4-methyl-6-(hydroxymethyl)phenolate(1-)]germanate (4)

A solution of $Ge(NMe_2)_4$ (0.562 g, 2.26 mmol) in diethyl ether (5 mL) was added dropwise into a solution of 3-*tert*-butyl-2-hydroxy-5-methylbenzyl alcohol (1.316 g, 6.78 mmol) in diethyl ether (60 mL) at −60 °C. The mixture was stirred and allowed to reach ambient temperature. The volatile solvent (approximately 3/4 of the solvent volume) was removed by slow evaporation under reduced pressure (10^{-1} mbar). A colorless precipitate occurred during evaporation of the solvent. The colorless solid was filtered off and washed with *n*-hexane (3 times 5 mL) to give germanate **4** after evaporating the volatile residues under reduced pressure (10^{-2} mbar). Yield: 1.006 g, 64%; mp 128–129 °C; ^{1}H NMR (500 MHz, CDCl$_3$, 25 °C, TMS): δ = 1.38 [s (broad), 27 H, C(CH_3)$_3$], 2.02 (s, 6 H, NCH_3), 2.23 [s (broad), 9 H, CH_3], 4.93 [s (broad), 6 H, CH_2], 6.60 [s (broad), 3 H, C$_6H_2$], 6.98 [s (broad), 3 H, C$_6H_2$], 7.47 ppm [s (broad), 3 H, OH/NH_2]; ^{13}C{^{1}H} NMR (125 MHz, CDCl$_3$, 25 °C, TMS): δ = 20.7 (CH_3), 30.1 [C(CH_3)$_3$], 34.8 [C(CH$_3$)$_3$], 35.7 (NCH_3), 66.7 (CH_2), 124.7 (C$_6$H$_2$), 126.8 (C$_6$H$_2$), 127.4 (C$_6$H$_2$), 127.6 (broad, C$_6$H$_2$), 139.3 (C$_6$H$_2$), 155.2 ppm (C$_6$H$_2$); ^{1}H ^{13}C{^{1}H} HSQC NMR (125 MHz, CDCl$_3$, 25 °C, TMS): δ = 1.38/29.9 [C(CH_3)$_2$], 2.02/35.6 (NCH_3), 2.23/20.7 (CH_3), 4.86/66.5 (CH_2), 6.52/125.9 (C$_6H_2$), 6.90/126.7 ppm (C$_6H_2$); ATR-FT-IR: 3268 (ν O–H), 3002 (ν C$_{aryl}$–H), 2948 (ν CH$_3$/CH$_2$), 2898 (ν CH$_3$/CH$_2$), 2861 (ν CH$_3$/CH$_2$), 2460 (ν N–H), 1607 (ν C═C), 1468 (δ CH$_2$), 1441 (δ CH$_2$), 1358 (δ CH$_3$), 1219 (ν C–O), 1144 (ν C–N), 1026 (ν C–C), 1001 (ν C–C), 859 (γ C$_6$H$_2$), 822 (γ C$_6$H$_2$), 693 (ν Ge–O), 619 (ν Ge–O), 550 and 525 and 507 and 442 cm^{-1} (O–Ge–O/Ge–O–Ge); CHN analysis calcd (%) for **4** (C$_{38}$H$_{57}$GeNO$_6$): C, 65.5; H, 8.3; N, 2.0; found: C, 64.8; H, 8.5; N, 1.9. Single crystals suitable for X-ray diffraction analysis were obtained by slow evaporation of the solvent at ambient temperature of a saturated solution of **4** in *n*-hexane.

4.5 Synthesis of phenolic resin/germanium dioxide hybrid materials by thermally induced twin polymerization in melt – HM-1

Compound **1** (1.776 g, 3.34 mmol) was polymerized at 200 °C under Ar atmosphere and treated at this temperature for 3 h. The obtained solid was washed with dichloromethane (3 times 10 mL) and dried under reduced pressure (10^{-1} mbar) in order to remove volatile by-products. The product **HM-1** is a yellow monolith composed of phenolic resin/GeO_2. Yield: 1.189 g, 67%; ^{13}C{^{1}H} CP-MAS NMR (100.6 MHz, 25 °C, TMS): δ = 35 (CH_2), 43 [N(CH_3)$_2$], 116 (C$_6H_3$/C$_6H_4$), 119 (C$_6H_3$/C$_6H_4$), 129 (C$_6H_3$/C$_6H_4$), 153 ppm (C$_6H_3$/C$_6H_4$); ATR-FT-IR: 3600–3100 (ν O–H), 3015 (ν C$_{aryl}$–H), 2921 (ν CH$_2$), 2361 (ν N–H), 1590 (ν C═C), 1455 (δ CH$_2$), 1227 (ν C–O), 1096 (ν C–N/C–C), 1015 (ν C–C), 810 (γ C$_6$H$_4$/C$_6$H$_3$), 750 (γ C$_6$H$_4$/C$_6$H$_3$), 506 and 451 cm^{-1} (O–Ge–O/Ge–O–Ge); CHN analysis (%) found: C, 53.8; H, 4.9; N, 2.6; EDX analysis (%) found: C, 60.5 ± 10.3; N, 5.0 ± 1.7; O, 22.9 ± 4.4; Ge, 11.6 ± 0.9. A yellow liquid (**Sub-1**, 0.083 g) condensed at the top of the reaction vessel during the polymerization process. NMR spectroscopic analysis of **Sub-1** revealed 2-[(dimethylamino)methyl]phenol as major product: ^{1}H NMR (500 MHz, CDCl$_3$, 25 °C, TMS): δ = 2.32 (s, 6 H, CH_3), 3.64 (s, 2 H, CH_2), 6.77 (td, H, C$_6H_4$, $^3J_{ortho}$ = 7.3 Hz, $^4J_{meta}$ = 1.0 Hz), 6.83 (dd, H, C$_6H_4$, $^3J_{ortho}$ = 7.9 Hz, $^4J_{meta}$ = 1.0 Hz), 6.95 (dd, H, C$_6H_4$, $^3J_{ortho}$ = 7.3 Hz, $^4J_{meta}$ = 1.9 Hz), 7.16 (td, H, C$_6H_4$, $^3J_{ortho}$ = 7.9 Hz, $^4J_{meta}$ = 1.9 Hz), 8.12 ppm (s (broad), H, OH); ^{13}C{^{1}H} NMR (125 MHz, CDCl$_3$, 25 °C, TMS): δ = 44.4 (CH_3), 62.8 (CH_2), 116.0 (C$_6$H$_4$), 118.9 (C$_6$H$_4$), 121.9 (C$_6$H$_4$), 128.2 (C$_6$H$_4$), 128.7 (C$_6$H$_4$), 158.0 ppm (C$_6$H$_4$); ^{1}H ^{13}C{^{1}H} HSQC NMR (125 MHz, CDCl$_3$, 25 °C, TMS): δ = 2.32/44.1 (NCH_3), 3.64/62.7 (CH_2), 6.79/118.8 (C$_6H_4$), 6.84/115.9 (C$_6H_4$), 6.97/128.4 (C$_6H_4$), 7.18/128.8 ppm (C$_6H_4$).

4.6 Synthesis of porous Ge@C material C-1 starting from HM-1

HM-1 (0.238 g) was carbonized under reducing conditions in a stove (deposited in a quartz glass tube) for 3 h with a final temperature of 800 °C (heating ramp of 10 K min^{-1}) under Ar/H_2 flux (95/5, 20 Lh^{-1}) to give **C-1** as metallic shiny black solid. Yield: 0.139 g; single point BET-surface area determined at p/p_0 = 0.150 ± 0.002: 470 m^2 g^{-1}; QSDFT analysis of the

isotherm revealed a micropore content of 61% for the pore volume of 0.259 $cm^3\ g^{-1}$; ATR-FT-IR: 745, 629, 529 and 473 cm^{-1}; CHN analysis (%) found: C, 59.6; H, 0.3; N, —; EDX analysis (%) found: Ge, 20.5 ± 1.0; crystalline Ge particle size of (27 ± 1) nm were determined by PXRD analysis applying the Scherer equation based on the (220) reflection of Ge ICDD no. C03-065-0333.

4.7 Synthesis of germanium dioxide material Ox-1 – starting from HM-1

HM-1 (0.272 g) was oxidized in a stove (deposited in a quartz glass tube) for 3 h with a final temperature of 800 °C (heating ramp of 10 K min^{-1}) under air flux (200 Lh^{-1}) to give **Ox-1** as colorless monolith. Yield: 0.075 g, single point BET-surface area determined at p/p_0 = 0.150 ± 0.002: 27 $m^2\ g^{-1}$, ATR-FT-IR: 850, 579, 546 and 513 cm^{-1}; the presence of hexagonal (α-quartz-like structure ICDD no. C00-036-1463) GeO_2 with a particle size of (47 ± 6) nm was determined by PXRD analysis applying the Scherer equation based on the (101) reflection.

4.8 Single crystal X-ray diffraction analyses

Crystallographic data of the compounds **1**·1/2 CH_2Cl_2, 8·**2**·17 CH_2Cl_2 and **4** were collected with an Oxford Gemini S diffractometer (CrysAlis RED Version 1.171.32.5 from Oxford Diffraction Ltd) using Cu-K_α radiation (λ = 1.54184 Å, **1**·1/2 CH_2Cl_2) or Mo-K_α (λ = 0.71073 Å, 8·**2**·17 CH_2Cl_2 and **4**) at 110 K, respectively. The single crystal X-ray diffraction analysis of compound **1**·1/2 CH_2Cl_2 was performed using Cu-K_α radiation due to the small size of its crystals causing poor reflectivity. The structures were solved by direct methods using SHELXS-2013 and refined by full matrix least-square procedures on F^2 using SHELXL-2013.[43] Absorption corrections were semi-empirical from equivalents. All non-hydrogen atoms were refined anisotropically and a riding model was employed in the refinement of hydrogen atom positions. The crystallographic data for **1**·1/2 CH_2Cl_2, 8·**2**·17 CH_2Cl_2 and **4** have been deposited at the Cambridge Crystallographic Data Centre as supplementary publications CCDC 1440866 (**1**·1/2 CH_2Cl_2), CCDC 1440864 (8·**2**·17 CH_2Cl_2) and CCDC 1440865 (**4**).

4.9 Electrode fabrication, cell assembly and electrochemical measurements

Ge@C samples, carbon black (CB, Super C65, TIMCAL), and carboxymethyl cellulose (CMC, Grade: 2200, Daicel Fine Chem Ltd) were mixed in the ratio 8 : 1 : 1 with deionized water using a Fritsch Pulverisette 7 classic planetary mill operated for one hour at 500 rpm. The aqueous slurries were coated onto Cu foil (9 μm, MTI Corporation) and then dried at 80 °C for 12 hours under vacuum. Electrochemical measurements were conducted in air tight coin-type cells assembled in an Ar-filled glove box (O_2 < 0.1 ppm, H_2O < 0.1 ppm) using elemental lithium as counter and reference electrode and a piece of glass fiber as separator (GF/D Whatman). 1 M $LiPF_6$ in a 1 : 1 mixture by wt. of ethylene carbonate (EC) and dimethyl carbonate (DMC) (Merck, battery grade) with 3% fluoroethylene carbonate (FEC, Hisunny Chemical Co., battery grade) was used as electrolyte. Galvanostatic cycling tests were carried out on a MPG2 multi-channel workstation (BioLogic). All electrochemical tests were conducted at ambient temperature.

Acknowledgements

We gratefully acknowledge financial support by the DFG, Forschergruppe 1497 "Organic–Inorganic Nanocomposites through Twin polymerization", and the Fonds der Chemischen Industrie for a fellowship (P. Kitschke). M. Walter and Prof. Dr M. V. Kovalenko thank the CTI Swiss Competence Centers for Energy Research (SCCER, 'Heat and Electricity Storage') for financial support. We thank N. Rüffer for TGA measurements and M. Weber for recording the Raman spectra. Prof. Dr S. Spange and Dr A. Seifert are acknowledged for access to the solid state NMR spectrometer and for fruitful discussions. The referees are acknowledged for helpful comments.

Notes and references

1 T. Ebert, A. Seifert and S. Spange, *Macromol. Rapid Commun.*, 2015, **36**, 1623–1639.
2 S. Grund, P. Kempe, G. Baumann, A. Seifert and S. Spange, *Angew. Chem., Int. Ed.*, 2007, **46**, 628–632.
3 S. Spange and S. Grund, *Adv. Mater.*, 2009, **21**, 2111–2116.
4 C. Leonhardt, S. Brumm, A. Seifert, G. Cox, A. Lange, T. Rüffer, D. Schaarschmidt, H. Lang, N. Jöhrmann, M. Hietschold, F. Simon and M. Mehring, *ChemPlusChem*, 2013, **78**, 1400–1412.
5 A. Mehner, A. Pohlers, W. Hoyer, G. Cox and S. Spange, *Macromol. Chem. Phys.*, 2013, **214**, 1000–1010.
6 A. Mehner, T. Rüffer, H. Lang, A. Pohlers, W. Hoyer and S. Spange, *Adv. Mater.*, 2008, **20**, 4113–4117.
7 C. Schliebe, T. Gemming, J. Noll, L. Mertens, M. Mehring, A. Seifert, S. Spange and H. Lang, *ChemPlusChem*, 2015, **80**, 559–567.
8 F. Böttger-Hiller, R. Lungwitz, A. Seifert, M. Hietschold, M. Schlesinger, M. Mehring and S. Spange, *Angew. Chem., Int. Ed.*, 2009, **48**, 8878–8881.
9 P. Kitschke, A. A. Auer, T. Löschner, A. Seifert, S. Spange, T. Rüffer, H. Lang and M. Mehring, *ChemPlusChem*, 2014, **79**, 1009–1023.
10 S. Spange, P. Kempe, A. Seifert, A. A. Auer, P. Ecorchard, H. Lang, M. Falke, M. Hietschold, A. Pohlers, W. Hoyer, G. Cox, E. Kockrick and S. Kaskel, *Angew. Chem., Int. Ed.*, 2009, **48**, 8254–8258.
11 C. Leonhardt, S. Brumm, A. Seifert, A. Lange, S. Csihony and M. Mehring, *ChemPlusChem*, 2014, **79**, 1440–1447.
12 J. Liu, K. Song, C. Zhu, C.-C. Chen, P. A. van Aken, J. Maier and Y. Yu, *ACS Nano*, 2014, **8**, 7051–7059.
13 S. Jin, N. Li, H. Cui and C. Wang, *ACS Appl. Mater. Interfaces*, 2014, **6**, 19397–19404.
14 G. H. Yue, X. Q. Zhang, Y. C. Zhao, Q. S. Xie, X. X. Zhang and D. L. Peng, *RSC Adv.*, 2014, **4**, 21450–21455.

15 N. Nitta, F. Wu, J. T. Lee and G. Yushin, *Mater. Today*, 2015, **18**, 252–264.
16 C.-M. Park, J.-H. Kim, H. Kim and H.-J. Sohn, *Chem. Soc. Rev.*, 2010, **39**, 3115–3141.
17 J. Hwang, C. Jo, M. G. Kim, J. Chun, E. Lim, S. Kim, S. Jeong, Y. Kim and J. Lee, *ACS Nano*, 2015, **9**, 5299–5309.
18 P. Kitschke, S. Schulze, M. Hietschold and M. Mehring, *Main Group Met. Chem.*, 2013, **36**, 209–214.
19 C. Stanciu, A. F. Richards, M. Stender, M. M. Olmstead and P. P. Power, *Polyhedron*, 2006, **25**, 477–483.
20 M. C. Etter, *Acc. Chem. Res.*, 1990, **23**, 120–126.
21 A. Biller, C. Burschka, M. Penka and R. Tacke, *Inorg. Chem.*, 2002, **41**, 3901–3908.
22 J. Parr, A. M. Z. Slawin, J. D. Woollins and D. J. Williams, *Polyhedron*, 1994, **13**, 3261–3263.
23 T. Baramov, K. Keijzer, E. Irran, E. Mösker, M.-H. Baik and R. Süssmuth, *Chem. – Eur. J.*, 2013, **19**, 10536–10542.
24 T. Steiner, *Angew. Chem., Int. Ed.*, 2002, **41**, 48–76.
25 R. Tacke, J. Heermann and B. Pfrommer, *Inorg. Chem.*, 1998, **37**, 2070–2072.
26 R. Tacke, J. Heermann and M. Pulm, *Organometallics*, 1997, **16**, 5648–5652.
27 *CRC Handbook of Chemistry and Physics*, Editor-in-chief D. R. Lide, CRC Press, Inc., 84th edn, 2004.
28 R. L. Bryson, G. R. Hatfield, T. A. Early, A. R. Palmer and G. E. Maciel, *Macromolecules*, 1983, **16**, 1669–1672.
29 B. D. Park and B. Riedl, *J. Appl. Polym. Sci.*, 2000, **77**, 1284–1293.
30 B. Ottenbourgs, P. Adriaensens, R. Carleer, D. Vanderzande and J. Gelan, *Polymer*, 1998, **39**, 5293–5300.
31 K. C. Klavetter, S. M. Wood, Y.-M. Lin, J. L. Snider, N. C. Davy, A. M. Chockla, D. K. Romanovicz, B. A. Korgel, J.-W. Lee, A. Heller and C. B. Mullins, *J. Power Sources*, 2013, **238**, 123–136.
32 C. Lastoskie, K. E. Gubbins and N. Quirke, *Langmuir*, 1993, **9**, 2693–2702.
33 C. Lastoskie, K. E. Gubbins and N. Quirke, *J. Phys. Chem.*, 1993, **97**, 4786–4796.
34 A. Macias-Garcia, M. A. Diaz-Diez, E. M. Cuerda-Correa, M. Olivares-Marin and J. Ganan-Gomez, *Appl. Surf. Sci.*, 2006, **252**, 5972–5975.
35 P. I. Ravikovitch and A. V. Neimark, *Langmuir*, 2006, **22**, 11171–11179.
36 P. I. Ravikovitch, A. Vishnyakov, R. Russo and A. V. Neimark, *Langmuir*, 2000, **16**, 2311–2320.
37 C. J. Rasmussen, A. Vishnyakov, M. Thommes, B. M. Smarsly, F. Kleitz and A. V. Neimark, *Langmuir*, 2010, **26**, 10147–10157.
38 M. Thommes, R. Kohn and M. Fröba, *Appl. Surf. Sci.*, 2002, **196**, 239–249.
39 M. Thommes, R. Kohn and M. Fröba, *J. Phys. Chem. B*, 2000, **104**, 7932–7943.
40 R. Withnall, I. R. Dunkin and R. Snaith, *J. Chem. Soc., Perkin Trans. 2*, 1994, 1973–1977.
41 Y. J. Wan and J. G. Verkade, *Inorg. Chem.*, 1993, **32**, 79–81.
42 N. U. Hofsløkken and L. Skattebøl, *Acta Chem. Scand.*, 1999, **53**, 258–262.
43 G. M. Sheldrick, *Acta Crystallogr., Sect. A: Fundam. Crystallogr.*, 2008, **64**, 112–122.